Nuclear Inst. and Methods in Physics Research, A 1040 (2022) 167099

Contents lists available at ScienceDirect

Nuclear Inst. and Methods in Physics Research, A

journal homepage: www.elsevier.com/locate/nima

An Alternating Phase Focusing injector for heavy ion acceleration

S. Lauber [a,b,c,*], S. Yaramyshev [a], M. Basten [a,b], K. Aulenbacher [a,b,c], W. Barth [a,b,c], C. Burandt [a,b], M. Droba [d], F. Dziuba [a,b], P. Forck [a], V. Gettmann [a], T. Kuerzeder [a,b], J. List [a,b,c], M. Miski-Oglu [a,b], H. Podlech [d], A. Rubin [a], M. Schwarz [d]

[a] GSI Helmholtz Center for Heavy Ion Research, Planckstraße 1, Darmstadt, 64291, Germany
[b] HIM Helmholtz Institute Mainz, Staudingerweg 18, Mainz, 55128, Germany
[c] KPH, Johannes Gutenberg University, Saarstraße 21, Mainz, 55122, Germany
[d] IAP, Goethe University, Frankfurt, Max-von-Laue-Str. 1, Frankfurt a.M., 60438, Germany

ARTICLE INFO

Keywords:
Heavy ion
Linear accelerator
Beam dynamics simulation
Continuous wave
Nonlinear beam dynamics
Alternating Phase Focusing

ABSTRACT

The new heavy ion superconducting continuous wave HElmholtz LInear ACcelerator (HELIAC) is under construction at GSI. A normal conducting injector, comprising an ECR ion source, an RFQ and a DTL, is recently in development. The new Interdigital H-mode DTL, presented in this paper, accelerates the heavy ion beam from 300 to 1400 keV/u, applying an Alternating Phase Focusing (APF) beam dynamics scheme. This APF section, consisting of two separately controlled tanks, has to provide for stable routine operation with assistance of dedicated beam diagnostics devices in the Intertank section. The installed quadrupole lenses and beam steerers installed there ensure full transmission in a wide range of input beam parameters.

1. Introduction

The Helmholtz Centre for Heavy Ion Research (GSI), with the Universal Linear Accelerator (UNILAC) as core of the accelerator facility [1], offers a rich environment for accelerator applications, as the linear heavy ion decelerator (HITRAP) [2], the UNILAC proton beam delivery [3,4] and the Laser Ion Generation, Handling and Transport (LIGHT) system for laser acceleration of protons and heavy ions [5]. Additionally, new linear accelerators are under construction: the HElmholtz LInear ACcelerator (HELIAC) [6–10] and the proton linac for the Facility for Antiproton and Ion Research at Darmstadt (FAIR) [11,12].

The HELIAC will compensate the demand for short pulse high intensity beams for FAIR [1,13] and the demand for long term continuous wave CW beam operation in particular for the GSI Super Heavy Element (SHE) research program. The requirements for FAIR has to be fulfilled by the existing UNILAC augmented by an upgraded post-stripper section [14–16], whilst the HELIAC will extend the rich selection of injector linacs at GSI as the first superconducting (SC) CW heavy ion linac, enabling further investigations and discoveries of new super heavy elements at GSI [17–19]. Meanwhile, the operation of SC CW accelerators has become a vital part of accelerator centers and its research fields around the world, as for spallation neutron sources or medium energy applications in material science, isotope generation and boron-neutron capture therapy [20–25].

The HELIAC project is a collaboration of GSI and the Helmholtz Institute Mainz (HIM) [26–28], under key support of the Goethe University Frankfurt (GUF) [8,29,30] and formerly in partnership with the Moscow Engineering Physics Institute (MEPhI) and the Moscow Institute for Theoretical and Experimental Physics (KI-ITEP) and JiNR-Dubna [31,32].

1.1. HELIAC

A normal conducting injector has to supply beam to the SC CW HELIAC (see Fig. 1). The 108 MHz injector features a dedicated Electron Cyclotron Resonance Source (ECR), a Radio Frequency Quadrupole (RFQ) and two normal conducting Interdigital H-mode (IH) DTL cavities, providing for a heavy ion beam at 1.4 MeV/u for the superconducting main linac [8]. The superconducting HELIAC is the most advanced part for the realization of this project, utilizing a new beam dynamics concept, called Equidistant Multigap Structure (EQUUS) [7], implemented to a string of 12 superconducting crossbar H-mode (CH) cavities operated at 217 MHz [29,33] mounted together in four cryostats, dedicated to a variable beam energy variation from 3.5 to 7.3 MeV/u (see Table 1).

Commissioning of the first SC cavity CH0 with beam has been performed successfully in 2017 [9,34]. The GSI High Charge State Injector (HLI) in operation has been temporarily used to deliver beam to a test cryomodule, where the strong capabilities of CH0 were demonstrated,

* Corresponding author at: HIM Helmholtz Institute Mainz, Staudingerweg 18, Mainz, 55128, Germany.
E-mail address: s.lauber@gsi.de (S. Lauber).

https://doi.org/10.1016/j.nima.2022.167099
Received 11 January 2022; Received in revised form 23 June 2022; Accepted 29 June 2022
Available online 5 July 2022

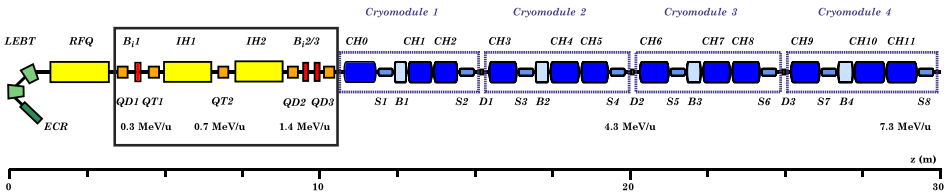

Fig. 1. Layout of the HELIAC comprising four cryomodules and its dedicated injector; this publication focuses on the injector DTL with its relevant components: Quadrupole Doublets (QD), Bunchers (B), Quadrupole Triplets (QT), Interdigital H-Mode Cavities (IH), Crossbar H-Mode Cavities (CH), Solenoids (S).

Table 1
General characteristics of the HELIAC accelerator.

Property	Value
Frequency	108.408 MHz (216.816 MHz[a])
Mass-to-charge ratio	≤6
Repetition rate	continuous wave
Beam current I	≤1 mA
Output energy E_{out}	3.5 to 7.3 MeV/u
Injector output energy E_{out}	300 keV/u
NC Cavities	2
SC Cavities	12

[a]The CH cavities operate at the second harmonic.

as the high mechanical stability, a high acceleration field gradient and variable output energy [35,36].

Previously, it has been discussed to use a CW capable replica of the HLI injector [37] for the HELIAC. The HLI injector cavity of IH type features a beam dynamics concept called Combined Zero Degree Structure (KONUS) [38]. Although the application of KONUS beam dynamics provides a very compact accelerator layout, in operation of HLI the beam quality has proven to be extremely sensitive to tank phase/voltage changes.

Recently, in place of a KONUS IH cavity, an Alternating Phase Focusing (APF) IH DTL has been proposed to be installed as HELIAC injector DTL. Therefore, two separately powered and tuned IH cavities were designed and should allow for eased commissioning and flexible robust routine operation. The Intertank section is equipped with further beam diagnostics devices, comprising a quadrupole triplet and beam steerers in order to make beam focusing and positioning standard operation [39–43]. Due to these additional beam line components, tuning, maintenance and most reliable injector operation is ensured.

1.2. Alternating Phase Focusing (APF)

APF is a beam dynamics concept that relies on the variation of synchronous phases during acceleration instead of using a constant synchronous phase along the DTL. The APF scheme utilizes negative as well as positive synchronous phases for beam acceleration, which provides for successive transverse and longitudinal RF-focusing inside a cavity. In general the optional use of quadrupoles is affected by boundary conditions as input beam emittance, available aperture, working frequency, acceleration gradient, transmission and the acceptable emittance growth. An embedded transverse RF-focusing through selection of an appropriate synchronous phase pattern allows for long quadrupole-free DTL sections compared to a conventional beam dynamics approach.

To provide for different phases in each gap, the DTL geometry is modified, different from typical DTLs such as the Wideroe $\beta\lambda/2$ pattern with β, the particle velocity as fraction of speed of light and λ, the RF wavelength. For the synchronous phase change between two neighboring gaps $\Delta\phi$, a modified cell length is yielded:

$$L_{\text{cell}} = \frac{\beta\lambda}{2} + \beta\lambda\frac{\Delta\phi}{360°} \tag{1}$$

Since APF focusing is a long known concept for sequential longitudinal–transverse focusing, proposed in 1953 [44,45], there is no consensus on how to select synchronous phases for each gap. Whilst a sinusoidal synchronous phase law using average accelerating field $\bar{E}$, field factor η and the amplitude of synchronous phase oscillation α was proposed by I. Fainberg [46],

$$\phi_i = \alpha\cos\left(\frac{\omega t}{n}\right) \tag{2}$$

$$n = \sqrt{\frac{\beta}{A(1-\beta^2)^{3/2}}} \tag{3}$$

$$A = \frac{\alpha}{\pi}\frac{e\bar{E}\eta\lambda}{mc^2} \tag{4}$$

different approaches have been investigated in the following years [47–50]:

- Irregular [51]
- Rectangular/step-function [52]
- Semi-sinusoidal [53,54]

The KONUS and EQUUS beam dynamics schemes can likewise be perceived as subtypes of the Alternating Phase Focusing concept, although both types do not target in omitting magnetic lenses.

Recently, a semi-sinusoidal APF channel has been designed and is in routine operation at the Heavy Ion Medical Accelerator center (HIMAC, Japan) [48,54]. Different accelerator based facilities are planning the application of an APF beam dynamics scheme, as the Muon Linac at J-PARC in Japan [55] or the Advanced Proton Therapy Facility (APTRON, China) [56].

In contrast, common acceleration phase patterns, typically employing a synchronous phase around −30°, yield only longitudinal beam focusing (accompanied by transverse defocusing) and dedicate the transverse beam focusing to magnetic lenses. Thus, magnetic lenses are installed inside drift tube cavities and offer a compact option to build an accelerator, as additional drifts are avoided. For Alvarez type cavities, the quadrupole lenses are commonly installed inside almost each drift tubes; Wideroe type cavities could also comprise multiple, bigger quadrupole duplets/triplets inside the tank drift tube. On the other hand, the emerging long tanks are more difficult to fabricate and to maintenance, where the repair and upgrade of inner-tank lenses is a highly challenging and time-consuming procedure. Beam accelerator units employing the APF focusing scheme are less affected by these challenges, as this makes it possible to provide for a layout without magnetic lenses or a limited number of quadrupoles outside a cavity. For HIMAC, a lens free region of 3.4 m was designed, providing for heavy ion acceleration from 400 keV/u to 4 MeV/u for a mass-to-charge ratio of 3 in routine linac injector operation for heavy ion cancer therapy.

1.3. Project overview

To deploy APF IH cavities for the HELIAC injector, major parts of the beam line are elaborated to provide for a compact design, as well as for beam matching to the adjacent SC accelerator section.

The initial IH-DTL beam parameters delivered by the RFQ are used as depicted in Table 2 [57]. The beam is convergent in the vertical plane and transversely divergent, with a beam spot width of ±2 mm

Table 2
Input beam parameters, as output of the RFQ [57].

Property	Value
W_{kin}	300 keV/u
I_{beam}	1 mA
Mass-to-charge ratio	6
Frequency	108.408 MHz
Distribution type	6D-Waterbag
No./ of macro particles	10 k
α_x	−1.228
β_x	0.16 mm/mrad
ϵ_x	31.8 mm mrad
$\epsilon_{x,normalized}$	0.81 mm mrad
α_y	+2.33
β_y	0.27 mm/mrad
ϵ_y	31.8 mm mrad
$\epsilon_{y,normalized}$	0.81 mm mrad
α_z	0
β_z	4.46 deg/(keV/u)
ϵ_z	62 deg keV/u

and angle of ±20 mrad, a bunch length of ±15° and energy spread of ±4 keV/u.

The normal conducting DTL injector linac design provides for five sections:

- Medium Energy Beam Transport (MEBT) (300 keV/u)
- APF-IH-Cavity-1 (300 to 700 keV/u)
- Intertank (700 keV/u)
- APF-IH-Cavity-2 (700 to 1400 keV/u)
- Matching Line to SC-linac (1400 keV/u)

The MEBT behind the RFQ is the matching section to the APF Cavity-1. The quadrupole doublet QD1 focuses the transversal divergent/convergent beam so that the rebuncher B_i1 provides for longitudinal focusing at full transmission to Cavity-1. The quadrupole triplet QT1 together with the buncher performs the 6D matching to the Cavity-1, which accelerates the beam from 300 to 700 keV/u. Another quadrupole triplet (QT2) in the Intertank region between the two cavities ensures for proper transverse focusing to the Cavity-2 (±5 mm). The design does not provide for an additional Intertank buncher, resulting in an utmost compact layout. Cavity-2 accelerates the beam to the final energy of 1400 keV/u. The Matching Line, equipped with two rebuncher cavities and two quadrupole doublets, provides for full beam matching to the superconducting HELIAC section.

For integration of the HELIAC into the GSI accelerator environment, a compact overall construction length of the injector chain is desired, requiring also short beam transport sections to be as compact as possible. Mainly the maximum quadrupole and buncher field strengths limit the compactness, since a too narrow beam could not be effectively focussed. Thus, long drift lengths are necessary to provide for suitable beam size by further beam propagation.

2. Design of an APF channel

During design of the APF beam dynamics scheme for a DTL, the synchronous phase in each RF-gap must be chosen accordingly. From a beam dynamics point of view the main task is to find the array of gap phases (i.e., synchronous phases) to achieve maximum beam acceleration with minimum emittance growth at full beam maximum transmission. A realistic DTL geometry can be derived from any synchronous phase array using Eq. (1).

As this design approach involves sequential transverse and longitudinal RF-focusing, it is essential to apply a beam dynamics code, which accounts 6D coupling of the particles positions and velocities in all room dimensions. A core strength of the chosen beam dynamics solver DYNAMION [58] is the inference of the 3D electromagnetic fields from an arbitrary DTL by given tube/gap geometry and gap voltages. In close collaboration with RF designers, providing for realistic cavity model implementation into electromagnetic simulations with CST-Studio Suite [59], the required gap voltages $\vec{U}$ could be obtained. Also, these CST-Studio Suite calculations allow for analysis of cavity characteristics (resonance frequency, peak fields, dissipated power etc.). In advanced calculation stages, the realistic 3D electromagnetic field mapping could also be ported from CST to DYNAMION.

In order to identify the synchronous phases in each gap $\vec{\phi}$, a random search strategy is adopted as a global optimization method, minimizing the performance function $f(\vec{\phi})$ (see Eq. (6)). This function addresses the linac beam requirements, namely beam focusing, emittance preservation and beam acceleration. The search boundaries $\vec{\phi}_{\min}$ and $\vec{\phi}_{\max}$ are iterative readjusted manually to shrink the search range in each gap, which gives fine control over the convergence in every design step. Simultaneously the voltage profile $\vec{U}$ was updated in accordance with the recent CST model.

A dedicated interface for global optimization of the cavity layout using multi-core parallel application of the beam dynamics code DYNAMION has been developed. The choice of a random search strategy allows for massively parallel computations, as no simulation depends on any other. All simulations and post-processes could be saved for later analysis. The procedure generally consists of following steps:

1. Selection of individual voltages per gap $\vec{U}$
2. Definition of synchronous phase limits $\vec{\phi}_{\min}$ and $\vec{\phi}_{\max}$
3. While $f > f_{\text{target}}$:
   (a) Generation of random array of phases $\vec{\phi}$ subject to $\vec{\phi}_{\min} < \vec{\phi} < \vec{\phi}_{\max}$
   (b) Generation of cavity geometry to yield above phases
   (c) Calculation of beam dynamics
   (d) Calculation of performance factor $f(\vec{\phi})$

This procedure results in the best cavity in terms of the performance function $f(\vec{\phi})$, which is mainly connected to the total emittance growth $\hat{\epsilon}$. To use the highest sensitivity on emittance growth, the smallest ellipses that surround 100 % of the particles are chosen to derive the total emittance growth, denoted as $\hat{\epsilon}$:

$$\hat{\epsilon} = \frac{\epsilon_{100\%,\text{out}}}{\epsilon_{100\%,\text{in}}} \tag{5}$$

The performance function considers both longitudinal and transverse emittance growth $\hat{\epsilon}_z$ and $\hat{\epsilon}_{x,y}$ as well as the cavity mean output energy E_{out}. Since a low emittance growth is required in both transverse planes uniformly, the transverse emittance growth parameter relevant for the calculation is used as $\hat{\epsilon}_{x,y} = \max(\hat{\epsilon}_x, \hat{\epsilon}_y)$. The performance function consists of three terms, accounting transverse and longitudinal emittance growth, as well as the output energy

$$f(\phi) = \left(\frac{\hat{\epsilon}_{x,y} - 1}{t_{x,y}}\right)^2 + \left(\frac{\hat{\epsilon}_z - 1}{t_z}\right)^2 + \frac{E_{\text{target}} - E_{\text{out}}}{t_{\text{E}}} \tag{6}$$

The energy related term in the performance function is intentionally not being squared to distinguish between higher and lower beam energies. Thus, higher output energies are allowed to be achieved, given the emittance growth stays reasonably low. The evaluation of the maximum envelope size inside the cavity was initially considered as performance criterion, but omitted, as the emittance growth is closely correlated to the transverse beam size and thus indirectly accounted for. Furthermore, it was decided to prioritize a lower longitudinal emittance growth against transversal, as an increased transverse beam emittance can be easily scraped, but more complicated dispersion sections would be necessary to remove particles with momentum deviation. Thus, the transverse tolerance parameter is chosen as $t_{x,y} = 1\%$ and the longitudinal is $t_z = 0.5\%$. The tolerance of the energy deviation is selected to be $t_{\text{E}} = 50$ keV.

In general, geometry layouts achieving 100 % transmission were taken into account for further analysis.

Table 3
Design parameters of Cavity-1.

Tank frequency	108.408 MHz
Acceleration gradient	3.0 MV/m
Input energy	300.0 keV/u
Output energy	700.3 keV/u
Length (beam dynamics)	1.3 m
Number of gaps	29
Aperture radius	9 mm

Table 4
Design parameters of Cavity-1.

Emittance Growth $\hat{\epsilon}_{100\%}$	
x, y (normalized)	5.0 %
z	8.0 %
Emittance Growth $\hat{\epsilon}_{90\%}$	
x, y (normalized)	3.5 %
z	1.3 %
Input Matching Parameters	
$\alpha_{x,y}$	0.89
$\beta_{x,y}$	0.55 mm/mrad
α_z	−0.03
β_z	4.63 deg/(keV/u)

As a part of the iterative global optimization, the input Twiss parameters were altered randomly within adjusted boundary values, analogous to the search strategy for the synchronous phases.

3. Reference beam dynamics

3.1. APF Cavity-1

Cavity-1 is the most critical part of the entire channel layout in terms of the performance function f. The beam is accelerated from the initial energy of 300 keV/u, applying an electric acceleration field gradient of 3 MV/m. In this energy region, the beam is highly sensitive to deformations of the longitudinal bunch shape, potentially resulting in increased emittance growth. Thus, this cavity had to be particularly carefully designed. The final geometric and beam dynamics characteristics are listed in Tables 3 and 4.

From preliminary design iterations it is decided to use a beam transition energy from Cavity-1 to Cavity-2 of 700 keV/u, balancing the requirements for low emittance growth and high energy gain, which results in an energy gain of 400 keV/u within Cavity-1 and 700 keV/u for Cavity-2. The gap lengths were fixed in early design stages to limit the surface field and thus to minimize thermal heating of the tubes. Thus, only the tube lengths can be varied freely to alter the cell length and therefore the synchronous phase. As a further constraint, a lower limit for the tube lengths was set to avoid too short tubes, which would otherwise cause problems regarding thermal heating, electric field linearity and manufacturing. The global optimization of the synchronous phase array yields a semi-sinusoidal phase profile along the cavity (see Fig. 2 and Table 5), reflecting generally a commonly observed pattern for APF cavities [49,53,54].

A transverse beam spot size less than 2/3 of the cavity aperture is obtained considering the maximum envelope, determined by calculation of all particle trajectories. During the design process it was intended to yield reasonable input Twiss parameters with a beam width of approx. ±4 mm, (±10 mrad) and approx. ±16° (±4 keV/u) (see Fig. 3). The transversal beam orientation and cavity output can be chosen arbitrary, since the beam is finally matched to the second cavity with a quadruple triplet. Longitudinally, the output orientation is strictly specified, as it is necessary to omit additional rebunching in the Intertank section. Therefore, the last gaps of this cavity are used to provide for a more narrow bunch lengths of approx. ±20° as input for

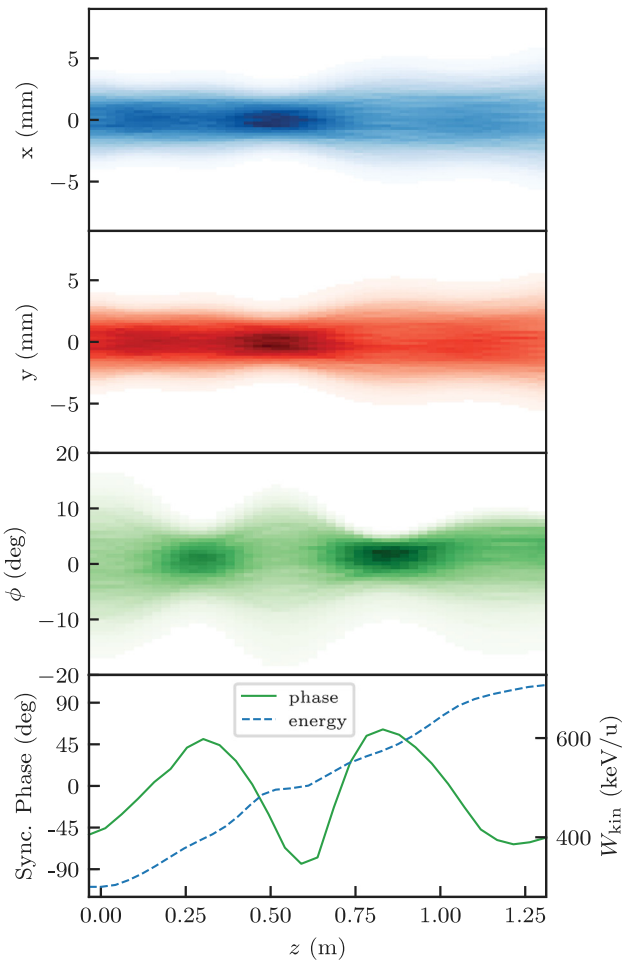

Fig. 2. Density encoded particle trajectories in the first tank Cavity-1 in all three planes and the corresponding synchronous phase.

Cavity-2 by choosing a synchronous phase of approx. −50° in the last gaps.

This is possible as the last gaps inflict the lowest changes to the overall beam dynamics within Cavity-1 and as the beam dynamics design of Cavity-2 is less demanding in terms of emittance growth at higher beam energy.

The beam dynamics calculations were verified and confirmed with two different, independent particle tracking solvers (DYNAMION and an internally developed code). The trajectories match with high precision. Steering effects below one millirad could be obtained from particle tracking simulation with the imported electromagnetic field of the actual cavity geometry from CST (including stems, tubes, etc.), for details on steering see Section 3.4.

The total transverse emittance growth is with 5 % in order of a usual channel (see Fig. 3), as well as the 8 % total longitudinal emittance growth. The emittance growth, especially longitudinally, is mainly present as a beam halo caused by non-linear 6D coupling. By considering 90 % of the particles, the emittance growth is negligible.

3.2. Intertank

The Intertank section between Cavity-1 and Cavity-2 is dedicated to additional transverse beam focusing, in order to confine the beam in the center of Cavity-2 and to design Cavity-2 for almost maximum acceleration. As there is no rebuncher in the Intertank, its length has to be determined in advance to fix the longitudinal Twiss parameters as

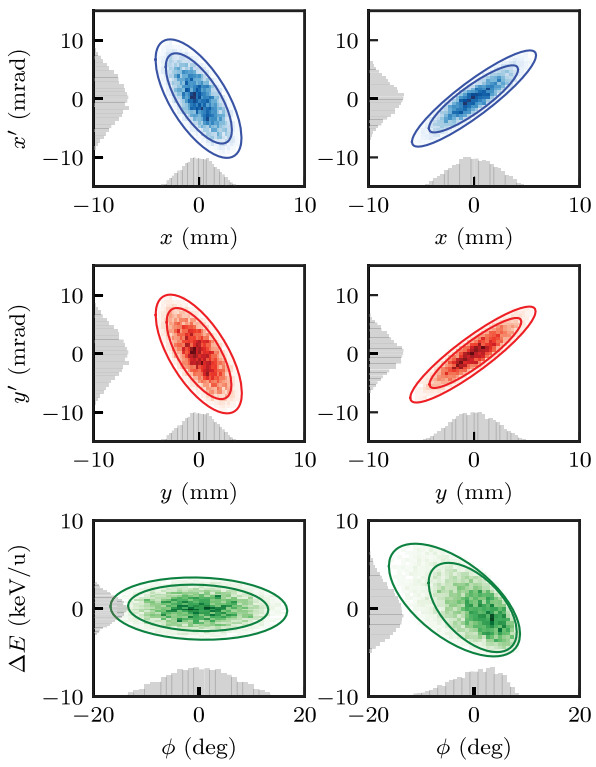

Fig. 3. Design particle distribution for Cavity-1: input particles (left), output phase space distribution (right), The ellipses enclose 90 % and 100 % of all particles, the color encodes the particle density.

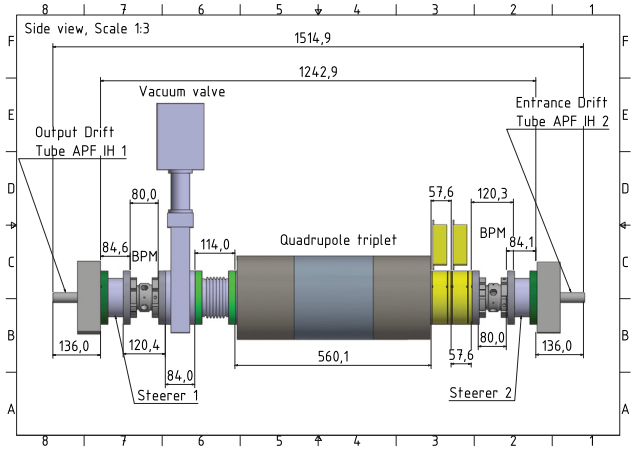

Fig. 4. Intertank section between Cavity-1 and Cavity-2 (all lengths in mm) including Beam Position Monitor (BPM).

input for Cavity-2. Thus, the fully equipped Intertank section has been composed in advance in order to start design of Cavity-2.

An Intertank section layout with the absolute essentials has been chosen. The 1.5 m long section consists of a quadrupole triplet, two beam steerers and two beam position monitors, as well as a standard vacuum section valve (see Fig. 4). The quadrupole triplet provides for transversal beam matching to Cavity-2 applying quadrupole gradients of about 20 T/m. The corresponding beam dynamics simulations are depicted in Fig. 8.

Certainly, the accelerator could have been built without an Intertank section, but early drafts of a one-tank layout were discarded, mitigating further technical risks. The drawbacks would have been the fabrication and installation of a long tank, a decreased tolerance to

Table 5
Beam dynamics design values of Cavity-1.

Cell No.	Phase (deg)	Voltage (kV)	Gap center (mm)
1	−53.5	46.7	24.5
2	−47.9	97.6	60.9
3	−33.3	108.4	99.5
4	−13.9	118.6	139.9
5	6.5	128.0	181.5
6	24.2	136.8	223.6
7	39.5	144.6	266.2
8	50.8	151.4	308.8
9	47.9	156.3	348.9
10	27.4	160.4	385.6
11	−0.2	163.3	421.5
12	−31.6	165.6	457.4
13	−66.0	166.8	493.2
14	−84.0	167.8	533.5
15	−78.1	168.4	579.8
16	−22.5	167.5	639.0
17	27.5	165.5	698.0
18	50.5	163.2	751.2
19	59.7	160.4	801.5
20	55.8	158.2	848.8
21	42.8	154.3	894.2
22	22.9	148.2	938.3
23	0.5	143.0	982.4
24	−22.8	136.7	1027.0
25	−47.6	129.5	1071.8
26	−59.4	120.6	1120.8
27	−62.3	110.1	1172.7
28	−58.1	97.8	1227.0
29	−51.1	46.4	1282.5

Table 6
Design parameters of Cavity-2.

Tank frequency	108.408 MHz
Acceleration gradient	3.1 MV/m
Input energy	700.3 keV/u
Output energy	1400.0 keV/u
Length (beam dynamics)	1.8 m
Number of gaps	27
Aperture radius	9 mm

synchronous phase deviations, a twice big to-be-optimized parameter space and the lack of beam instrumentation, foreseen in the designed Intertank section. The design with two separate resonators enables the operation with two amplifiers, which offer independent phase and amplitude controls of the two cavities, allowing for compensation of eventual synchronous phase mismatch at the entrance of the second cavity, which prevents an accumulation of phase deviations along the whole channel. In addition, the quadrupole triplet and beam steerers also contribute to improved and reliable CW routine operation, an absolute necessity for accelerator facility operation with different ions and mass-to-charge ratios for multiple users in a time-sharing model.

3.3. APF Cavity-2

The beam dynamics design of Cavity-2 is less demanding, as the output beam rigidity of 0.9 T m is 50 % higher than for Cavity-1 (see Table 6). In any case, too long drift tubes, inefficient for cooling, had to be avoided. The optimization of the Cavity-2 synchronous phase array has been performed applying the same algorithm as for Cavity-1, yielding a different synchronous phase structure along the cavity (see Fig. 5 and Table 7) with a rapid jump from negative to positive synchronous phases followed by a minor synchronous phase oscillation around 0°. This pattern is caused by different input Twiss parameters than for Cavity-1 (see Table 8), which has a longitudinal canonical and transversal convergent beam as input. In contrast, the synchronous phase pattern of Cavity-2 must provide a longitudinal beam divergence and a transversal convergence at its exit.

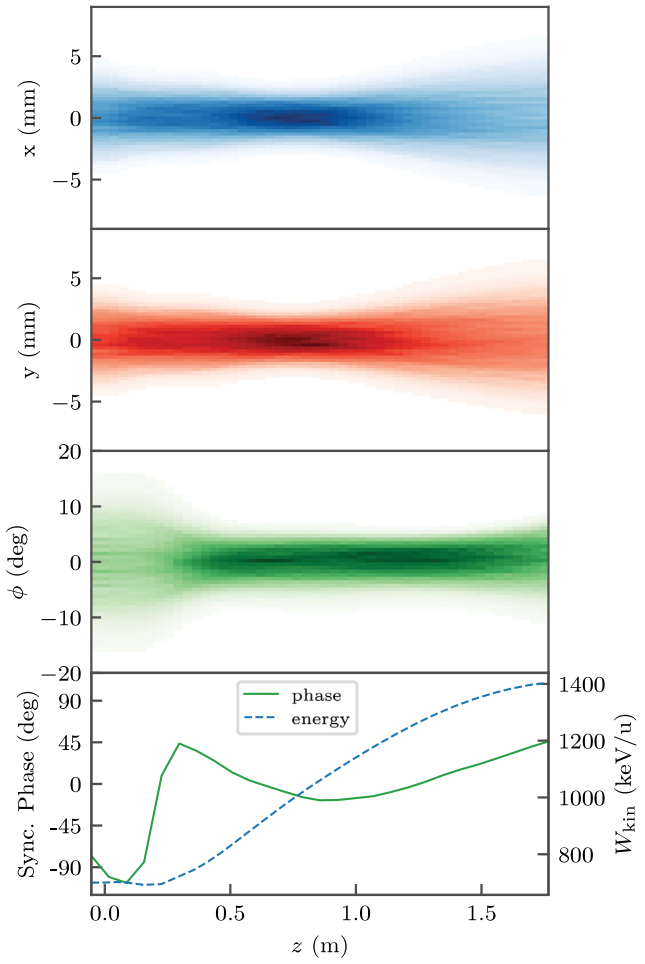

Fig. 5. Density encoded particle trajectories in the second tank Cavity-2 in all three planes and the corresponding synchronous phase.

Another notable aspect is the occurrence of a synchronous phase of −110° in the between drift tube 2 and drift tube 3. This is empirically found to yield the lowest emittance growth within Cavity-2, but was not expected, as a phase below −90° is unusual because it leads to deceleration of the beam. This phenomena was carefully investigated and is discussed in the following. The rapid phase change leads to an almost canonical bunch orientation longitudinally at 0.5 m with a narrow beam length below 10°. The compact beam is then suitable for acceleration with synchronous phases around 0°. Thus, the beam is accelerated until the beam gets too wide transversely. Until the exit, few positive synchronous phases refocus the beam transversely, which provides for longitudinal defocusing, allowing for a location of the following bunchers more close to the tank exit.

The observation of phases below −90° can be addressed by a two-gap model. The beam is accelerated by using of the RF acceleration field, introducing the lowest bunch deformation in the linear region of the RF wave and the highest deformation on the crest of the RF wave. The acceleration gain of the bunch is proportional to $\Delta E \propto \cos(\phi_i)$ and is zero at a synchronous phase of −90°, where the small-angle approximation could be made and minimal deformation is introduced to the beam. Together with the adjacent gap an acceleration/deformation of $\Delta E \propto \cos(\phi_i) + \cos(\phi_{i+1})$ is introduced (neglecting the short drift in between the two neighboring gaps). The decelerating phases and its neighboring one are about −110° and −70°. Thus, considering $\Lambda = 20°$, the previous expression can be rewritten as

$$\Delta E \propto \cos(-90° + \delta\phi - \Lambda) + \cos(-90° + \delta\phi + \Lambda), \tag{7}$$

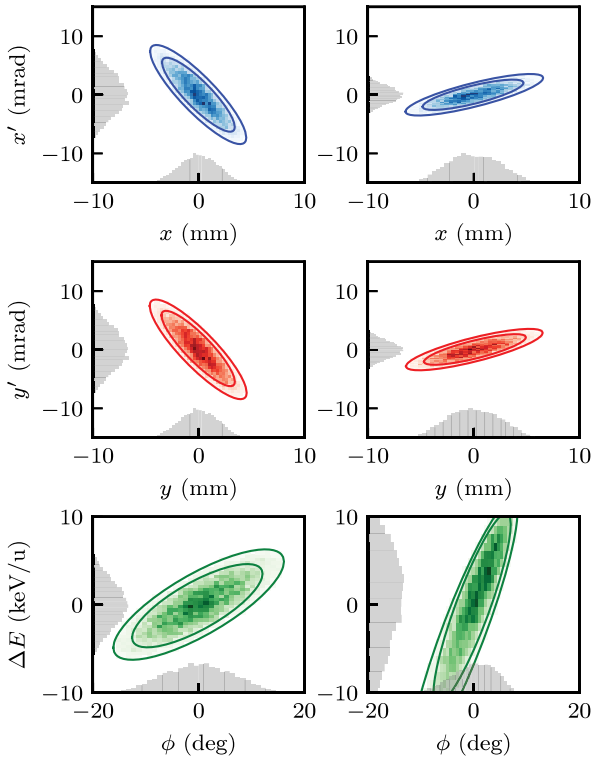

Fig. 6. Design particle distribution for Cavity-2: input particles (left), output phase space distribution (right), The ellipses enclose 90 % and 100 % of all particles, the color encodes the particle density.

Table 7
Beam dynamics design values of Cavity-2.

Cell No.	Phase (deg)	Voltage (kV)	Gap center (mm)
1	−77.7	62.5	26.6
2	−100.6	132.7	73.4
3	−106.9	151.1	125
4	−84.4	173.3	184.9
5	9.2	196.5	266
6	43.7	214.7	330.9
7	35.6	228.2	383.8
8	24.9	239.6	436.8
9	12.6	249.7	490.3
10	3.7	257.6	546.2
11	−2.5	263.8	604.2
12	−8.5	267.8	663.5
13	−14.3	268.8	724.2
14	−17.7	268	787
15	−17.4	265.6	852.3
16	−15.4	260.8	919.5
17	−13.4	253.8	987.8
18	−9	244.8	1058.2
19	−3.9	233.7	1130
20	2.3	221.2	1203.3
21	9.4	206.6	1278
22	15.6	189.5	1353.3
23	21	171.9	1429
24	27.2	153.2	1505.8
25	33.6	133.1	1583.3
26	40.1	111.9	1661.3
27	45.9	51.5	1739.4

and particles in vicinity with phase deviation $\delta\phi$ from the reference particle. By using the addition theorem $\sin(\alpha + \beta) + \sin(\alpha - \beta) = 2\sin(\alpha)\cos(\beta)$, Eq. (7) can be rewritten as

$$\Delta E \propto 2 \cdot \sin(\delta\phi) \cdot \cos(\Lambda). \tag{8}$$

Table 8
Design parameters of Cavity-2.

Emittance Growth $\hat{\epsilon}_{100\%}$	
x, y (normalized)	2.7 %
z	1.9 %
Emittance Growth $\hat{\epsilon}_{90\%}$	
x, y (normalized)	0.0 %
z	0.0 %
Input Matching Parameters	
$\alpha_{x,y}$	1.7
$\beta_{x,y}$	1.2 mm/mrad
α_z	1.31
β_z	4.27 deg /(keV/u)

It is apparent, that by this set of phases a linear beam focusing is achieved, with efficiency $cos(\Lambda = 20°) \approx 94\%$ of an ideal lens combination operated at −90°, −90°. The field gradient in the first gaps is about 50 % of the maximum gradient (in the center of the cavity): the effect of deceleration is minor, whereas early beam quality degradation could be even amplified within the following gaps. Thus, the beam is not overfocused and the phase transition to positive phases is smoothed with this unusual phase combination, preventing problems with thermal load and peak surface fields. The inflection of the RF pulse below −90° compensates the oppositely inflected RF pulse above −90° down streams and prevents emittance growth. Multiple approaches limiting the search space to the standard −90° resulted in a decreased beam quality. It has been decided to use a design in favor of high beam quality.

The output Twiss parameters are well adapted to allow for a short matching section to the superconducting HELIAC (see Fig. 6), which was imposed during synchronous phase array optimization. It has been ensured, that the longitudinal Twiss parameters provide for a most divergent beam to allow a buncher position close to the Cavity-2 output, reducing the overall length of the adjacent matching section. The demand for longitudinal divergence at Cavity-2 output has to be balanced with the necessity for a short bunch to limit the resulting emittance growth. Remarkably, the major part of emittance growth in the output plane is caused by particles being stretched away from the bunch center. In general, more complex distortion patterns are expected instead. This pattern eases matching to the superconducting section of HELIAC as the effective longitudinal emittance is low.

3.4. Steering effects

Due to the alternating mounting of the stems in both cavities, an electric dipole field component is present in each gap. It was therefore mandatory to investigate the impact of dipole fields components on beam transport and the resulting steering effect. For this realistic 3D electromagnetic field map within the cavity geometry has been imported from CST to DYNAMION.

Beam tracing simulations were performed to investigate steering effects within each cavity. The trajectories of reference particles in each cavity are shown in Fig. 7. The steering effect in Cavity-1 results in a negligibly small beam displacement of up to approx. 0.1 mm and 0.16 mrad in vertical direction. For Cavity-2 a higher displacement of 0.6 mm and −0.15 mrad is calculated. In general, this steering effect could be reduced with injection of an inclined beam. For Cavity-2 an input beam with 0.05 mm offset and 0.45 mrad angle has been found. The introduction of this small vertical inclination provides for a minor beam displacement behind Cavity-2 to below 0.1 mm and 0.06 mrad as well.

The two of already foreseen Intertank steerer magnets could be used to compensate steering effects within Cavity-2. Thus, the layout with two independent cavities even taking dipole component into account already demonstrates its benefit for safe routine DTL operation.

Table 9
Final design parameters and beam dynamics results for the whole channel.

Property	Value
Beam transmission	100 %
Input beam energy	300.0 keV/u
Output beam energy	1408.0 keV/u
Mean beam spot radius	4 mm
Max beam spot radius	7 mm
Emittance Growth $\hat{\epsilon}_{90\%}$	
x	5.0 %
y	5.0 %
z	3.0 %
Emittance Growth $\hat{\epsilon}_{100\%}$	
x	23.0 %
y	23.0 %
z	17.0 %

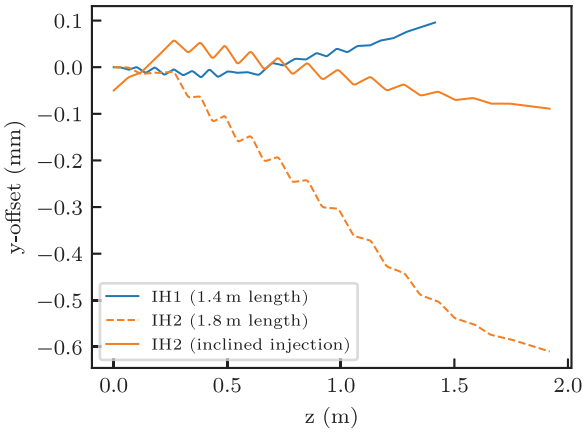

Fig. 7. Steering of reference particle in both cavities.

3.5. Full line simulations

The end-to-end beam dynamics simulation including all matching section is presented in Fig. 8. The MEBT from RFQ to Cavity-1 has been designed for a length of 1.8 m, the Matching Line, from Cavity-2 to the SC section, is 3.5 m long. The initial Twiss parameters are selected as depicted in Table 2.

The rebuncher B_i1 in the MEBT already causes a significant part of the total longitudinal emittance growth, mainly due to the combination of low beam energy and high phase length in the rebuncher, which makes the bunch susceptible to longitudinal deformations due to its low beam energy. A nonlinear deformed beam is delivered as input to Cavity-2, instead of a uniformly distributed bunch, which has been used during previous design stages. Since the cavity sensitivity to such changes is low, no additional emittance growth is observed.

The rebunchers $B_i2/3$ and the two quadrupole doublets QD2/3 in the Matching Line provide for longitudinal and transversal matching to the SC linac section. For this interconnected simulation using all beam transport elements, a particle transmission of 100 % is obtained for the whole line.

The APF channel provides for low emittance growth of approx. 20 % in each phase plane for the total emittance $\hat{\epsilon}$ (see Table 9).

With a net length (Cavities + Intertank) of 4.5 m the CW-IH-APF-DTL is 26 % longer compared to the existing HLI KONUS-type IH cavity operated at 25 % duty factor.

3.6. Beam dynamics error studies

For the two cavities the impact of potential perturbations during fabrication, assembly, and operation was investigated.

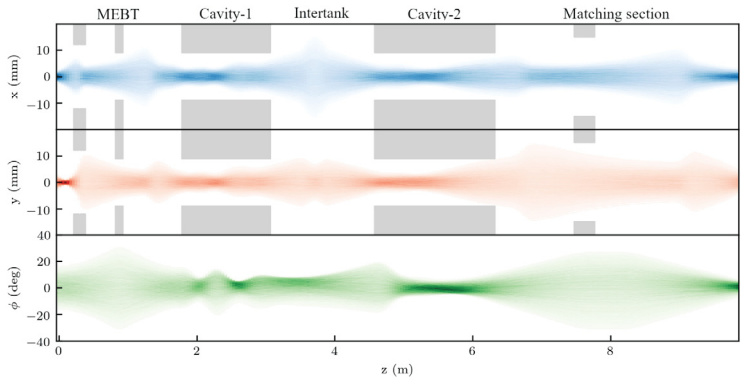

Fig. 8. End to end simulation of the whole channel from RFQ output to SC CH input. The particle density is encoded as color. The matching sections to the IH (left) and to the SC CH section (right) are included. The gray blocks indicate the aperture of the cavities and magnets; the maximum free aperture is 20 mm.

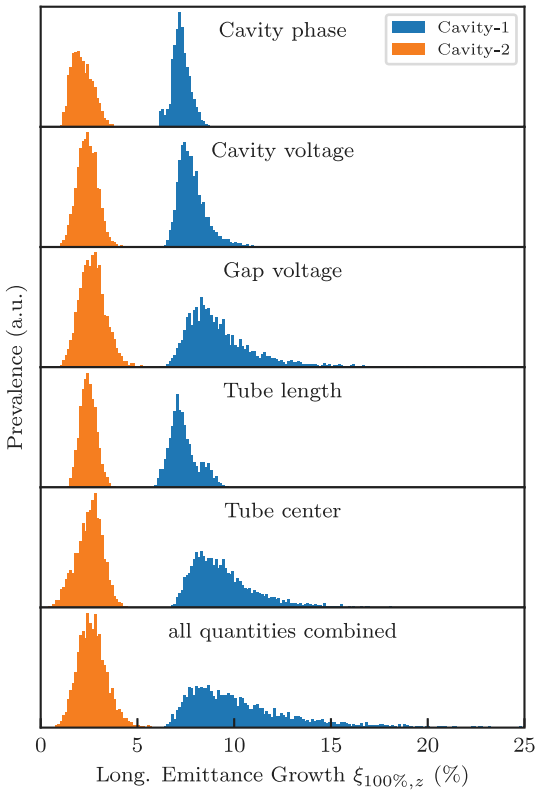

Fig. 9. Perturbation influence on longitudinal emittance growth (≈4000 simulations per histogram).

The influence of a deviation of drift tube length, caused by fabrication error has been investigated, as well as the installation accuracy of the stem/drift tube (i.e., tube center). Both properties effectively shift the adjacent gap centers and thus the synchronous phase. These synchronous phase changes inflict phase and energy changes, influencing the further beam transport, which affects finally the output beam quality.

Furthermore, the voltage in each individual gap has been varied, leading to different beam acceleration. In reality, the voltage inaccuracy is caused by either misplacement of tubes or different surface and geometric conditions compared to simulations [48].

Additionally, the phase and amplitude stability of the cavity is investigated, which could be perturbed by the RF power supply. A coupling between perturbations of cavity voltage (scaling the voltages in each gap equally) and cavity phase must be assumed, but the actual impact cannot be determined in detail.

Table 10
Assumed standard deviation for perturbation analysis.

Variable	Standard deviation σ
Tube center	200 µm
Tube length	100 µm
Gap voltage	2.0%
Cavity voltage	0.2%
Cavity phase	0.2°

For the further investigations it has been assumed that the perturbation variables are considered independently of each other. In general, these variables potentially can be coupled, in particular geometric variables to the electric field distribution. For investigations of coupling, time-consuming electromagnetic field simulations should be carried out, which is not feasible to be performed along with thousands of beam dynamics simulations.

All perturbations are sampled from a Gaussian distribution with standard deviation σ as depicted in Table 10. Each tube and gap is altered by an individual random value. The perturbation analysis is performed considering the total emittance growth $\hat{\epsilon}_z$, the emittance growth $\hat{\epsilon}_{90\%,z}$ is so low that it is negligible and thus not presented.

The results of perturbation analysis and its influence on the longitudinal emittance growth is depicted in Fig. 9. For each histogram approximately 4000 simulations have been performed.

The RF-phase and -voltage, as well as the tube length deviation, has impact on the longitudinal emittance growth of Cavity-1, nine out of ten of those simulation runs yield an emittance growth $\hat{\epsilon}_z \leq 9\%$, whereas the median and its standard deviation are $\hat{\epsilon}_z = (7.0 \pm 0.4)\%$. The tube center and gap voltage perturbation yield a more significant impact on the emittance growth, nine out of ten of the simulations are below $\hat{\epsilon}_z \leq 12\%$, the median is approximately $\hat{\epsilon}_z = (9 \pm 1)\%$. Additionally to the independent perturbations random combining all previous perturbations types has been investigated, where nine out of ten of those simulations yield $\hat{\epsilon}_z \leq 15\%$ with a median of $\hat{\epsilon}_z = (10 \pm 2)\%$. Disadvantageous combinations of tube center and gap voltage deviation are the main cause for this growth.

For Cavity-2, all calculations show emittance growth below 5 %. The main contributors to emittance growth are identified and has to be considered during the future fabrication and assembly. As initially mentioned, the $\hat{\epsilon}_{90\%}$ emittance growth remains negligible low for the perturbation analysis of the beam core, but also the presented total emittance growth of $\hat{\epsilon}_z$ values will not affect the operation considerably.

In addition to the influence on the beam quality, the perturbations could influence the output Twiss parameters of the beam. In accordance with the investigation on beam emittance growth, the corresponding Twiss parameters of the total emittance (the smallest ellipse enclosing 100 % of the particles) were analyzed during perturbation

Table 11
Standard deviation σ of cavity output Twiss parameters.

Perturbation source	$\sigma(\hat{\alpha}_{x,y})$	$\sigma(\hat{\beta}_{x,y})$[a]	$\sigma(\hat{\alpha}_z)$	$\sigma(\hat{\beta}_z)$[b]
Cavity-1				
Cavity phase	0.04	0.03	0	0.02
Cavity voltage	0.08	0.05	0.02	0.1
Gap voltage	0.12	0.08	0.09	0.18
Tube length	0.04	0.03	0.02	0.02
Tube center	0.12	0.07	0.07	0.16
All quantities combined	0.18	0.11	0.11	0.27
Cavity-2				
Cavity phase	0.02	0.02	0.02	0.01
Cavity voltage	0.04	0.04	0.05	0.03
Gap voltage	0.07	0.09	0.13	0.09
Tube length	0.02	0.02	0.02	0.01
Tube center	0.05	0.07	0.06	0.05
All quantities combined	0.09	0.11	0.16	0.11

[a]In m.
[b]In deg u/keV.

analysis. The standard deviation σ of the Twiss parameters is listed in Table 11 for each cavity. The highest deviations occur for both cavities with all quantities combined. Transversely, the Twiss parameters are $\hat{\alpha}_{\text{trans.}} = (-2.1 \pm 0.2)$ and $\hat{\beta}_{\text{trans.}} = (3.1 \pm 0.1)$ m. The transverse deviations could be compensated with the quadrupole lenses. Longitudinally, the orientation is mainly influenced by the perturbations of gap voltages and tube centers with $\hat{\alpha}_{\text{long.}} = (-2.11 \pm 0.15)$ and $\hat{\beta}_{\text{trans.}} = (-2.11 \pm 0.20)$ deg u/keV. As the operational parameters cavity phase and cavity voltage inflict only minor deviation (below 0.1), the Twiss parameters remain highly constant after fabrication of the cavity.

3.7. Impact of RF & thermal cavity layout on beam dynamics

The geometric, RF and thermal cavity design is elaborated with CST Studio Suite. An overview of its main values is given in Table 12. As the water-cooled cavities have to be CW capable, considerable efforts must be made with regard to the thermal design of the cavity (see Fig. 10). The heat load of a specific tube is governed by the variable length of the tube and its stem position on the girder, as well as the individual surface current, which is different along the cavity due to the specific resonance eigenmode (i.e., H_{11}). The part of the cavity, that heats up most in RF operation, are the fringe tubes with a maximum temperature of 413 K, which, due to the girder structure, is not as efficient coolable as the other drift tubes. The minimum and maximum tube lengths were constrained during beam dynamics design to prevent excessive heating. The tube lengths in Cavity-1 were limited from 16 to 60 mm and in Cavity-2 from 20 to 80 mm. Mechanical simulations under thermal load predict that the longitudinal displacement of the tubes due to thermal expansion will be less than 200 μm, as assumed in the perturbation analysis (see Table 10). The resulting emittance growth for Cavity-1 in nine out of ten of the perturbation simulations are below $\hat{\epsilon}_z \leq 12\,\%$, the results corresponding to Cavity-2 indicated emittance growth below 5 %.

Furthermore, a perturbation of the electric acceleration fields from the beam dynamics design values can lead to additional emittance growth. On one hand, the beam dynamics calculations were constantly updated by realistic field values from CST. On the other hand, to reduce eventual field perturbations from frequency tuner operation, three tuners are operated inside a cavity instead of two. With this design, the field perturbations are predicted to remain below 2 % even for maximum tuner displacement.

The electromagnetic design of the cavities yielded a Kilpatrick value of 2.5. Advanced experience from operation of DTL cavities, in particular at GSI, makes us confident that operation with such a Kilpatrick criterion is feasible.

A detailed report on the RF and thermal design of the cavities is beyond the scope of this paper and is published in [60].

Table 12
Final RF parameters.

Property	Cavity-1	Cavity-2
Design frequency	108.408 MHz	108.408 MHz
Number of gaps	29	27
Effective length L_{eff}	1.3 m	1.8 m
Length (outer cavity)	1.5 m	2.0 m
Electric peak field E_{Peak}	2.5 Kilpatrick	2.5 Kilpatrick
Length (inner wall-to-wall)	1.4 m	1.9 m
RF-power (100 % duty cycle)	20 kW	48 kW
Quality factor Q_0	19000	22000
Shunt impedance Z_0	690 MΩ/m	425 MΩ/m
Max. temperature	≈413 K	≈441 K
Accelerating gradient	3.0 MV/m	3.1 MV/m
Drift tube aperture radius	9 mm	9 mm
Drift tube outer radius	14 mm	17 mm

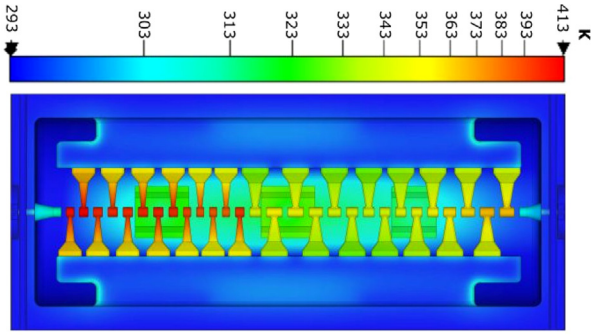

Fig. 10. Surface temperature inside Cavity-1. The peak temperature is strongly influenced by the choice of tube and gap lengths, obtained during beam dynamics design.

4. Conclusion & outlook

A continuous wave heavy ion accelerator section comprising two independently operated Interdigital H-mode cavities separated by an Intertank section, equipped with a quadrupole triplet, has been designed applying the Alternating Phase Focusing beam dynamics scheme. This enables the absence of magnetic lenses within the cavity. The newly proposed focusing scheme was obtained by means of global optimization of a cavity geometry, which shall provide for a 3 MV/m acceleration gradient. Thus, a dedicated phase law for beam matching was found for the two accelerating structures, in particular enabling a compact matching sections. The beam emittance growth in each cavity is sufficiently low in all phase planes, i.e., less than 5 %. Additionally, the cavities were found to cause minor steering of the beam below 500 μm and 0.2 mrad, the influence on beam dynamics is therefore negligible. The RF properties have been simulated, the geometry design has to prevent thermal limitations of the cavities. The independently powered cavities allow for eased commissioning, maintenance, operation and potential future upgrades. The cavities are currently tendered, fine adjustments in accordance with the cavity model used by the vendor are foreseen. The IH cavities will be deployed as the main part of the room temperature CW heavy-ion injector linac of the HELIAC accelerator.

Declaration of competing interest

The authors declare that they have no known competing financial interests or personal relationships that could have appeared to influence the work reported in this paper.

Data availability

Data will be made available on request.

References

[1] W. Barth, W. Bayer, L. Dahl, L. Groening, S. Richter, et al., Upgrade program of the high current heavy ion UNILAC as an injector for FAIR, Nucl. Instrum. Methods Phys. Res. A 577 (1) (2007) 211–214, http://dx.doi.org/10.1016/j.nima.2007.02.054.

[2] F. Herfurth, Z. Andelkovic, W. Barth, W. Chen, L. Dahl, et al., The HITRAP facility for slow highly charged ions, Phys. Scr. T166 (2015) 014065, http://dx.doi.org/10.1088/0031-8949/2015/T166/014065.

[3] W. Barth, A. Adonin, S. Appel, P. Gerhard, M. Heilmann, et al., Heavy ion linac as a high current Proton beam injector, Phys. Rev. ST Accel. Beams 18 (2015) 050102, http://dx.doi.org/10.1103/PhysRevSTAB.18.050102.

[4] A. Adonin, W. Barth, F. Heymach, R. Hollinger, H. Vormann, et al., Production of high current Proton beams using complex H-rich molecules at GSI, Rev. Sci. Instrum. 87 (2016) 02B709, http://dx.doi.org/10.1063/1.4934620.

[5] S. Busold, A. Almomani, V. Bagnoud, W. Barth, S. Bedacht, et al., Shaping laser accelerated ions for future applications – the LIGHT collaboration, Nucl. Instrum. Methods Phys. Res. A 740 (2014) 94–98, http://dx.doi.org/10.1016/j.nima.2013.10.025.

[6] W. Barth, R. Hollinger, A. Adonin, M. Miski-Oglu, U. Scheeler, et al., LINAC developments for heavy ion operation at GSI and FAIR, J. Instrum. 15 (12) (2020) T12012, http://dx.doi.org/10.1088/1748-0221/15/12/t12012.

[7] S. Minaev, U. Ratzinger, H. Podlech, M. Busch, W. Barth, Superconducting, energy variable heavy ion linac with constant β, multicell cavities of CH-type, Phys. Rev. ST Accel. Beams 12 (2009) 120101, http://dx.doi.org/10.1103/PhysRevSTAB.12.120101.

[8] M. Schwarz, S. Yaramyshev, K. Aulenbacher, W. Barth, M. Basten, et al., Reference beam dynamics layout for the SC CW heavy ion HELIAC at GSI, Nucl. Instrum. Methods Phys. Res. A (2019) 163044, http://dx.doi.org/10.1016/j.nima.2019.163044.

[9] W. Barth, K. Aulenbacher, M. Basten, M. Busch, F. Dziuba, et al., First heavy ion beam tests with a superconducting multigap CH cavity, Phys. Rev. Accel. Beams 21 (2018) 020102, http://dx.doi.org/10.1103/PhysRevAccelBeams.21.020102.

[10] M. Yarmohammadi Satri, A.M. Lombardi, F. Zimmermann, Multiobjective genetic algorithm approach to optimize beam matching and beam transport in high-intensity Hadron linacs, Phys. Rev. Accel. Beams 22 (5) (2019) 054201, http://dx.doi.org/10.1103/PhysRevAccelBeams.22.054201.

[11] R. Berezov, O. Delferriere, J. Fils, Y. Gauthier, R. Hollinger, et al., Status of high intensity Proton injector for facility for antiproton and ion research, Rev. Sci. Instrum. 90 (12) (2019) 123309, http://dx.doi.org/10.1063/1.5127820.

[12] U. Ratzinger, R. Tiede, H. Podlech, G. Clemente, B. Hofmann, et al., The 70 MeV p-injector design for FAIR, in: Proc. AIP'05, Vol. 773, 2005, pp. 249–253, http://dx.doi.org/10.1063/1.1949539.

[13] W. Barth, A. Adonin, C. Düllmann, M. Heilmann, R. Hollinger, et al., High brilliance uranium beams for the GSI FAIR, Phys. Rev. ST Accel. Beams 20 (2017) 050101, http://dx.doi.org/10.1103/PhysRevAccelBeams.20.050101.

[14] W. Barth, A. Adonin, C.E. Düllmann, M. Heilmann, R. Hollinger, et al., U^{28+}-intensity record applying a H_2-gas stripper cell, Phys. Rev. ST Accel. Beams 18 (4) (2015) 040101, http://dx.doi.org/10.1103/PhysRevSTAB.18.040101.

[15] A. Adonin, R. Hollinger, Beam brilliance investigation of high current ion beams at GSI heavy ion accelerator facility, Rev. Sci. Instrum. 85 (2014) 02A727, http://dx.doi.org/10.1063/1.4833931.

[16] S. Yaramyshev, H. Vormann, A. Adonin, W. Barth, L. Dahl, et al., Virtual charge state separator as an advanced tool coupling measurements and simulations, Phys. Rev. ST Accel. Beams 18 (2015) http://dx.doi.org/10.1103/PhysRevSTAB.18.050103.

[17] J. Khuyagbaatar, A. Yakushev, C.E. Düllmann, D. Ackermann, L.L. Andersson, et al., Search for elements 119 and 120, Phys. Rev. C 102 (6) (2020) 064602, http://dx.doi.org/10.1103/PhysRevC.102.064602.

[18] M. Block, D. Ackermann, K. Blaum, C. Droese, M. Dworschak, et al., Direct mass measurements above uranium bridge the gap to the island of stability, Nature 463 (7282) (2010) 785–788, http://dx.doi.org/10.1038/nature08774.

[19] J. Khuyagbaatar, A. Yakushev, C.E. Düllmann, D. Ackermann, L.L. Andersson, et al., $^{48}Ca + ^{249}Bk$ Fusion reaction ceading to element $Z = 117$: Long-lived α-decaying ^{270}Db and discovery of ^{266}Lr, Phys. Rev. Lett. 112 (17) (2014) 172501, http://dx.doi.org/10.1103/PhysRevLett.112.172501.

[20] R. Laxdal, K. Fong, M. Laverty, A. Mitra, R. Poirier, et al., Recent progress in the superconducting RF program at TRIUMF/ISAC, Phys. C: Superconductivity 441 (2006) 13–20, http://dx.doi.org/10.1016/j.physc.2006.03.096.

[21] O. Brunner, S. Calatroni, E. Ciapala, M. Eshraqi, R. Garoby, et al., Assessment of the basic parameters of the CERN superconducting Proton linac, Phys. Rev. ST Accel. Beams 12 (7) (2009) 070402, http://dx.doi.org/10.1103/PhysRevSTAB.12.070402.

[22] S. Polozov, A. Fertman, High-energy Proton beam accelerators for subcritical nuclear reactors, At. Energ. 113 (2013) 192–200, http://dx.doi.org/10.1007/s10512-012-9616-4.

[23] Z. Wang, Y. He, H. Jia, W. Dou, W. Chen, et al., Beam commissioning for a superconducting Proton linac, Phys. Rev. Accel. Beams 19 (2016) 120101, http://dx.doi.org/10.1103/PhysRevAccelBeams.19.120101.

[24] I. Mardor, O. Aviv, M. Avrigeanu, D. Berkovits, A. Dahan, et al., The soreq applied research accelerator facility (SARAF): Overview, research programs and future plans, Eur. Phys. J. A 54 (5) (2018) 91, http://dx.doi.org/10.1140/epja/i2018-12526-2.

[25] L.V. Grigorenko, B.Y. Sharkov, A.S. Fomichev, A.L. Barabanov, W. Barth, et al., Scientific program of DERICA – Prospective accelerator and storage ring facility for radioactive ion beam research, Phys.-Usp. 62 (7) (2019) 675–690, http://dx.doi.org/10.3367/ufne.2018.07.038387.

[26] W. Barth, K. Aulenbacher, M. Basten, M. Busch, F. Dziuba, et al., Superconducting CH-cavity heavy ion beam testing at GSI, J. Phys. Conf. Ser. 1067 (2018) 052007, http://dx.doi.org/10.1088/1742-6596/1067/5/052007.

[27] F. Dziuba, K. Aulenbacher, W. Barth, M. Basten, C. Burandt, et al., Further RF measurements on the superconducting 217 MHz CH demonstrator cavity for a CW linac at GSI, J. Phys. Conf. Ser. 1350 (2019) 012185, http://dx.doi.org/10.1088/1742-6596/1350/1/012185.

[28] S. Lauber, K. Aulenbacher, W. Barth, M. Basten, C. Burandt, et al., A dynamic collimation and alignment system for the Helmholtz Linear Accelerator, Rev. Sci. Instrum. 92 (11) (2021) 113306, http://dx.doi.org/10.1063/5.0069824.

[29] H. Podlech, U. Ratzinger, H. Klein, C. Commenda, H. Liebermann, et al., Superconducting CH structure, Phys. Rev. ST Accel. Beams 10 (2007) http://dx.doi.org/10.1103/PhysRevSTAB.10.080101.

[30] G. Clemente, U. Ratzinger, H. Podlech, L. Groening, R. Brodhage, et al., Development of room temperature crossbar-H-mode cavities for Proton and ion acceleration in the low to medium beta range, Phys. Rev. ST Accel. Beams 14 (11) (2011) http://dx.doi.org/10.1103/PhysRevSTAB.14.110101.

[31] M. Gusarova, W. Barth, S. Yaramyshev, M. Miski-Oglu, M. Basten, et al., Design of the two-gap superconducting re-buncher, J. Phys. Conf. Ser. 1067 (2018) 082005, http://dx.doi.org/10.1088/1742-6596/1067/8/082005.

[32] A.E. Aksent'ev, K.A. Aliev, I.A. Ashanin, Y.A. Bashmakov, A.A. Blinnikov, et al., Modeling of Proton beam dynamics in an accelerator-driver at 600-1000 MeV and investigation of the electrodynamic characteristics of accelerating cavities, At. Energ. 117 (5) (2015) 347–356, http://dx.doi.org/10.1007/s10512-015-9932-6.

[33] F. Dziuba, M. Busch, M. Amberg, H. Podlech, C. Zhang, et al., Development of superconducting crossbar-H-mode cavities for Proton and ion accelerators, Phys. Rev. ST Accel. Beams 13 (4) (2010) http://dx.doi.org/10.1103/PhysRevSTAB.13.041302.

[34] S. Yaramyshev, K. Aulenbacher, W. Barth, M. Basten, M. Busch, et al., Advanced approach for beam matching along the multi-cavity SC CW linac at GSI, J. Phys. Conf. Ser. 1067 (2018) 052005, http://dx.doi.org/10.1088/1742-6596/1067/5/052005.

[35] P. Gerhard, W. Barth, L. Dahl, A. Orzhekhovskaya, K. Tinschert, et al., Commissioning of a new CW radio frequency quadrupole at GSI, in: Proc. IPAC'10, 2010, pp. 741–743, URL http://accelconf.web.cern.ch/AccelConf/IPAC10/papers/mopd028.pdf.

[36] U. Ratzinger, Effiziente Hochfrequenz-Linearbeschleuniger FÜR Leichte Und Schwere Ionen, IAP, Goethe University, Frankfurt am Main, Germany, 1998, URL https://books.google.de/books?id=zh7UMAAACAAJ, Habilitation.

[37] W. Barth, K. Aulenbacher, M. Basten, F. Dziuba, V. Gettmann, et al., A superconducting CW-linac for heavy ion acceleration at GSIX, EPJ Web Conf. 138 (2017) 01026, http://dx.doi.org/10.1051/epjconf/201713801026.

[38] R. Tiede, U. Ratzinger, H. Podlech, C. Zhang, G. Clemente, KONUS beam dynamics designs using H-mode cavities, in: Proc. HB'08, 2008, pp. 223–230, URL http://accelconf.web.cern.ch/AccelConf/HB2008/papers/wgb11.pdf.

[39] S. Lauber, K. Aulenbacher, W. Barth, F. Dziuba, J. List, et al., Longitudinal phase space reconstruction for a heavy ion accelerator, Phys. Rev. Accel. Beams 23 (11) (2020) 114201, http://dx.doi.org/10.1103/PhysRevAccelBeams.23.114201.

[40] B. Walasek-Hoehne, C. Andre, P. Forck, E. Guetlich, G. Kube, et al., Scintillating screen applications in accelerator beam diagnostics, IEEE Trans. Nucl. Sci. 59 (5, 2) (2012) 2307–2312, http://dx.doi.org/10.1109/TNS.2012.2200696.

[41] T. Giacomini, S. Barabin, P. Forck, D. Liakin, V. Skachkov, Development of residual gas profile monitors at GSI, in: AIP Conf. Proc., in: Beam Instrumentation Workshop 2004, Vol. 732, 2004, pp. 286–293, http://dx.doi.org/10.1063/1.1831159.

[42] T. Sieber, W. Barth, F. Dziuba, A. Feschenko, P. Forck, et al., Bunch shape measurements at the GSI CW-linac prototype, in: Proc. IPAC'18, 2018 pp. 2091–2094, URL http://jacow.org/ipac2018/papers/wepak006.pdf.

[43] A. Feschenko, Methods and instrumentation for bunch shape measurements, in: Proc. PAC'01, 2001, pp. 517–521, http://dx.doi.org/10.1109/PAC.2001.987557.

[44] J.H. Adlam, A method of simultaneously focusing and accelerating a beam of Protons, AERE GP/M (146) (1953).

[45] M.L. Good, Phase-reversal focusing in linear accelerators, Phys. Rev. 92 (1953) 538, Berkeley Radiation Laboratory report.

[46] I.B. Fainberg, Alternating phase focusing, in: Proc. Conf. on High Energy Accelerators, CERN, Geneva, Switzerland, 1956, http://dx.doi.org/10.5170/CERN-1956-025.91.

[47] I.M. Kapchinskiy, Theory of Linear Resonance Accelerators, Harwood Academic Pub, United States, 1985, URL http://inis.iaea.org/search/search.aspx?orig_q=RN:19051333.

[48] V. Kapin, Y. Iwata, S. Yamada, Effects of field distortions in IH-APF linac, in: Proc. RuPAC, 2004, pp. 459–461.

[49] U. Niedermayer, T. Egenolf, O. Boine-Frankenheim, P. Hommelhoff, Alternating-phase focusing for dielectric-laser acceleration, Phys. Rev. Lett. 121 (21) (2018) 214801, http://dx.doi.org/10.1103/PhysRevLett.121.214801.

[50] G.N. Kropachev, Focusing of charged particles in linear accelerator, (Ph.D. thesis), ITEP, Moscow, 1994, UDK:621.384.64.

[51] D.A. Swenson, Alternating phase focused linacs, in: Particle Accelerators, Vol. 7, 1976, pp. 61–67, URL https://s3.cern.ch/inspire-prod-files-b/b4d96e9e3994558372a231ffb378d8b5.

[52] T. Hattori, K. Yamamoto, N. Hayashizaki, H. Kashiwagi, Y. Takahashi, et al., A study of a test APF-IH type linac as an injector for cancer therapy, Nucl. Instrum. Methods Phys. Res. B 188 (1) (2002) 221–224, http://dx.doi.org/10.1016/S0168-583X(01)01101-6.

[53] M. Otani, T. Mibe, M. Yoshida, K. Hasegawa, Y. Kondo, et al., Interdigital H-mode drift-tube linac design with alternative phase focusing for Muon linac, Phys. Rev. Accel. Beams 19 (4) (2016) 040101, http://dx.doi.org/10.1103/PhysRevAccelBeams.19.040101.

[54] Y. Iwata, S. Yamada, T. Murakami, T. Fujimoto, T. Fujisawa, et al., Alternating-phase-focused IH-DTL for an injector of heavy-ion medical accelerators, Nucl. Instrum. Methods Phys. Res. A 569 (3) (2006) 685–696, http://dx.doi.org/10.1016/j.nima.2006.09.057.

[55] Y. Nakazawa, H. Iinuma, Y. Iwata, Y. Iwashita, M. Otani, et al., Development of inter-digital H-mode drift-tube linac prototype with alternative phase focusing for a Muon linac in the J-PARC Muon G-2/EDM experiment, J. Phys. Conf. Ser. 1350 (2019) 012054, http://dx.doi.org/10.1088/1742-6596/1350/1/012054.

[56] X. Li, Y. Pu, F. Yang, X. Xie, Q. Gu, et al., RF design and study of a 325 MHz 7 MeV APF IH-DTL for an injector of a Proton medical accelerator, Nucl. Sci. Tech. 30 (9) (2019) 135, http://dx.doi.org/10.1007/s41365-019-0657-4.

[57] M. Vossberg, A. Schempp, C. Zhang, W. Barth, L. Dahl, The new GSI HLI-RFQ for CW-operation, in: Proc. LINAC'11, 2011, pp. 494–496.

[58] S. Yaramyshev, W. Barth, L. Groening, A. Kolomiets, T. Tretyakova, Development of the versatile multi-particle code DYNAMION, Nucl. Instrum. Methods Phys. Res. A 558 (1) (2006) 90–94, http://dx.doi.org/10.1016/j.nima.2005.11.018.

[59] CST MicroWave studio, 2021, https://www.cst.com, Accessed: 2022-07-06.

[60] M. Basten, K. Aulenbacher, W. Barth, C. Burandt, F. Dziuba, et al., Continuous wave interdigital H-mode cavities for alternating phase focusing heavy ion acceleration, Rev. Sci. Instrum. 93 (6) (2022) 063303, http://dx.doi.org/10.1063/5.0094859.